Controlled Immobilization of a Palladium Complex/Laccase Hybrid into a Macrocellular Siliceous Host

Fangfang Yang, Pierre Rousselot-Pailley, Cendrine Nicoletti, A. Jalila Simaan, Bruno Faure, Elise Courvoisier-Dezord, Agnès Amouric, Yolande Charmasson, Rénal Backov, Thierry Tron, et al.

ChemPlusChem

Research Article
doi.org/10.1002/cplu.202300156

Chemistry Europe
European Chemical Societies Publishing

www.chempluschem.org

Controlled Immobilization of a Palladium Complex/Laccase Hybrid into a Macrocellular Siliceous Host

Fangfang Yang,[a, b] Pierre Rousselot-Pailley,[a] Cendrine Nicoletti,[a] A. Jalila Simaan,[a] Bruno Faure,[a] Elise Courvoisier-Dezord,[a] Agnès Amouric,[a] Yolande Charmasson,[a] Rénal Backov,[c] Thierry Tron,[a] and Yasmina Mekmouche*[a]

This study investigates the site-directed immobilization of a hybrid catalyst bearing a biquinoline-based-Pd(II) complex (**1**) and a robust laccase within cavities of a silica foam to favor veratryl alcohol oxidation. We performed the grafting of **1** at a unique surface located lysine of two laccase variants, either at closed (**1**⊂UNIK$_{157}$) or opposite position (**1**⊂UNIK$_{71}$) of the enzyme oxidation site. After immobilization into the cavities of silica monoliths bearing hierarchical porosity, we show that catalytic activity is dependent on the orientation and loading of each hybrid, **1**⊂UNIK$_{157}$ being twice as active than **1**⊂UNIK$_{71}$ (203 TON vs 100 TON) when operating under continuous flow. These systems can be reused 5 times, with an operational activity remaining as high as 40%. We show that the synergy between **1** and laccase can be tuned within the foam. This work is a proof of concept for controlling the organization of a heterogeneous hybrid catalyst using a Pd/laccase/silica foam.

Introduction

Improving the selective and efficient generation of pure intermediates to produce pharmaceuticals, agrochemicals and fine chemicals is one of the most intensely pursued objectives in organic synthesis.[1] Metal-based catalysts, especially those used for the oxidation of organic substrates, are still scarce, expensive, and hardly recyclable so that there is an urgent need to optimize their use in the prospect of a sustainable economy. Efforts have been made to design transition metal catalysts enabling an efficient activation of O_2 and/or a good selectivity of the reaction by tuning the ligand/metal combination.[2] However, their scope remains limited and experimental conditions still often deal with harsh conditions.[3] Transition metals are found at the heart of redox enzymes.[4] Beyond exhibiting exquisite (enantio)selectivities, these enzymes are sustainable catalysts working in benign conditions.[5] Constant progress is made toward circumventing drawbacks for their use in process applications such as low operational stabilities and high production costs. Moreover, their reaction repertoire is constantly enriched with the implementation of directed evolution technics[6] and the development of chemical modifications to tune the protein surface.[7] In this respect, hybrid chemoenzymatic catalysts' that combine enzymes and nanometallic species or non-noble metal complexes have attracted growing attention for selective chemical transformations (Heck reaction, alcohol oxidation…), as they appear as promising sustainable alternatives to traditional catalysts. These hybrid systems overcome the limitations encountered separately in each field,[8] allowing several reaction steps to be performed while limiting further purification steps. Compared to mono-catalytic processes, synergies obtained with hybrids lead to higher turnover numbers (TON) and selectivities. In addition, the development of material technology has enabled the design and synthesis of a plethora of 3D catalyst supports with tunable pore size and surface functionalization.[9] In this endeavor, heterogeneous chemoenzymatic catalysis is as an emerging field explored for the benefit of multiple possible combinations of enzymes, chemical catalysts and materials.[10] In this direction, the main challenges ahead are: *i*) obtaining a functional compatibility of the catalysts in the same reaction media; *ii)* maintaining a cohabitation of catalysts within the material (operational activity); *iii*) controlling the spatial distribution and configuration of the active centers relative to each-others; *iv*) evaluating the support influence over a specific reaction; *v*) improving the system robustness (enzyme stability, lixiviation, metal leaching).

In several examples, enzymes themselves are converted into heterogeneous support upon treatment with cross-linking agents e.g. glutaraldehyde to form cross-linked aggregates (CLEAS). Metal nanoparticles (Cu, Pd, Pt) can be immobilized in these networks, providing hybrid catalysts largely documented by Palomo,[11] Backwall[12] and Zare[13] groups. Bifunctional systems depicting performant one-pot chemoenzymatic con-

[a] *Dr. F. Yang, Dr. P. Rousselot-Pailley, Dr. C. Nicoletti, Dr. A. J. Simaan, Dr. B. Faure, E. Courvoisier-Dezord, Dr. A. Amouric, Y. Charmasson, Dr. T. Tron, Dr. Y. Mekmouche*
Aix Marseille Univ
Centrale Marseille
CNRS, iSm2
13397 Marseille (France)
E-mail: y.mekmouche@univ-amu.fr
[b] *Dr. F. Yang*
College of Chemistry and Chemical Engineering
Yantai University
264005 Yantai (China)
[c] *Prof. R. Backov*
Université de Bordeaux, CNRS, CRPP, UMR5031
115 Avenue Albert Schweitzer
33600 Pessac (France)

Supporting information for this article is available on the WWW under https://doi.org/10.1002/cplu.202300156

version of substrates have been also explored through a confinement within exogenous materials such as porous imine molecular cages,[14] mesocellular silica foams,[15] MOFs,[16] zeolite materials[17] or mesoporous metals.[18] These developments on model reactions can be considered as proofs of concept of the interplay between chemical and biological partners within the same host. All these approaches while confining the catalysts within micro/mesoporous voids are bearing several severe drawbacks, especially for flow catalysis such as accessibility of the catalytic sites, low diffusion kinetics and high molecular hindrance considering the fluid hydrodynamics.[19] Meanwhile, random orientations of anisotropic enzyme molecules with respect to the material surface can however dramatically alter their integrity and efficiency, making the support worth to consider as a partner in the catalytic process.[20] It seems therefore wise to include ways of controlling the spatial distribution of each partner of the catalysis i.e. the enzyme, the metal and the material as early as possible in the design of the hybrid.

We recently achieved a site-directed immobilization of a fungal laccase into glutaraldehyde activated Si(HIPE) monoliths (High internal Phase Emulsion).[21] We have used monolithic hosts bearing hierarchical porosity (micro- meso-macroporosties) where all the above-mentioned penalties are vanished as far as it can be, all the catalytic sites being accessible ate ease.[19,21] Laccase (EC 1.10.3.2) is a robust biocatalyst, which active sites are composed of two copper-containing centers: a surface located T1 Cu^{II} center responsible for the oxidation of substrate and a trinuclear copper T2/T3 center (TNC) responsible for the reduction of O_2 into H_2O.[22] Selectively decorating the inner surface of the foam with variants containing a unique solvent-exposed lysine located either near (K_{157}) or opposite (K_{71}) to the T1 substrate oxidation site named as $UNIK_{157}$ and $UNIK_{71}$ respectively, lead to tune the catalytic efficiency of the immobilized laccases.[21]

We have previously shown that an electron transfer (ET) can be established between a water-soluble biquinoline-based Pd(II) complex and the fungal laccase LAC3 (Scheme 1A).[23] During the selective oxidation of veratryl alcohol (VA) into veratryl aldehyde, LAC3 associates the regeneration of Pd(II) to the four-electron reduction of O_2 into H_2O. Thus, under homogeneous conditions, the association of LAC3 with the Pd(II)-complex results in a significant increase in the catalytic efficiency of the complex under mild conditions (25 °C, water, atm pressure).[23]

Here, we present a monolithic well-defined heterogeneous chemoenzymatic catalyst bearing hierarchical porosity built on an oriented immobilization of a robust laccase and a transition-metal-based complex into silica foam and its use for the aerobic oxidation of alcohol (Scheme 1B&C). We used a bi-functional Pd(II)-biquinoline complex (**1**) based on a ligand with two aldehyde functions (L) to immobilize monofunctionalizable laccase variants within a macrocellular silica-based foam. By controlling the grafting point at the enzyme's surface we modify the organization of the artificial active site that the enzyme/Pd(II)-complex/silica-matrix interface forms. The modulation of alcohol oxidation activity obtained is discussed in relation to differential orientations of the hybrid catalyst.

Results and Discussion

Synthesis and characterization of complex [(L)$PdCl_2$] (1)

We have previously described a bimolecular catalytic system combining the O_2-reducing power of the laccase with the catalytic power of a Pd(II) nitrogen-based water-soluble complex (Scheme 1A).[23] To prepare a graftable version of the biquinoline Pd(II) complex we synthesized ligand L by a simple esterification of the previously reported acid-containing ligand followed by a mild cerium(IV) ammonium nitrate acetal deprotection adapted from Ates et al.[24] (Figure S1). The subsequent metalation of the ligand was performed with $Pd(CH_3CN)_2Cl_2$ in dichloromethane. Characterization of the complex in solution (elementary analysis, UV-Vis, NMR) agrees with the structure of **1**. Slow diffusion of diethylether into a saturated complex **1** solution in CH_2Cl_2 afforded crystals suitable for single crystal X ray diffraction analysis (Figure S2, Table S1). The crystal structure of **1** reveals that the central Pd(II) ion is four-coordinated in a distorted square-planar environment by the two N atoms from the chelating 2,2′-biquinoline ligand and two Cl anions. This structure is comparable to other Pd based biquinoline complexes.[25]

Production of homogeneous Pd(II) complex-Laccase hybrids

Two UNIK variants, $UNIK_{71}$ and $UNIK_{157}$, were independently covalently grafted to complex **1** via a previously described reductive alkylation procedure.[26,27] The resulting Pd(II) complex functionalized enzymes (respectively labelled as **1**⊂$UNIK_{71}$ and **1**⊂$UNIK_{157}$) ideally bear a free aldehyde group available for a post-functionalization (Scheme 1B) although the possibility of forming dimers during grafting exists. Time-course of the reductive alkylation was followed by SDS-PAGE for both enzymes (Figure S3). No evidence of oligomerization or protein loss was observed for both laccase variants during grafting reaction. After desalting and buffer exchange (ultrafiltration), the recovery yield was estimated to be min. 85% (Table 1). The efficiency of the functionalization was evaluated both from the ratio of the characteristic charge transfer bands at 610 nm for the T1 Cu(II) site of laccase ($\varepsilon_{610nm} = 5.6\times10^3\ M^{-1}cm^{-1}$) and at 340 nm for the Pd(II) complex ($\varepsilon_{340nm} = 2.7\times10^4\ M^{-1}cm^{-1}$) observed in the UV-Vis spectra of hybrids (Figure 1A) as by ICP-MS (Table 1).

N-terminal sequencing of the hybrids was conducted to exclude a possible alkylation of the N-terminus during functionalization. Several rounds of Edman degradation on both **1**⊂$UNIK_{71}$ and **1**⊂$UNIK_{157}$ attested that the N-terminal amine is free.

Specific activities of complex **1** grafted variants toward ABTS oxidation, a common laccase substrate, were found comparable to those of non-modified enzymes (Table 1).

The electron spin resonance (ESR) spectroscopic features of hybrids were found similar to those of the original variants

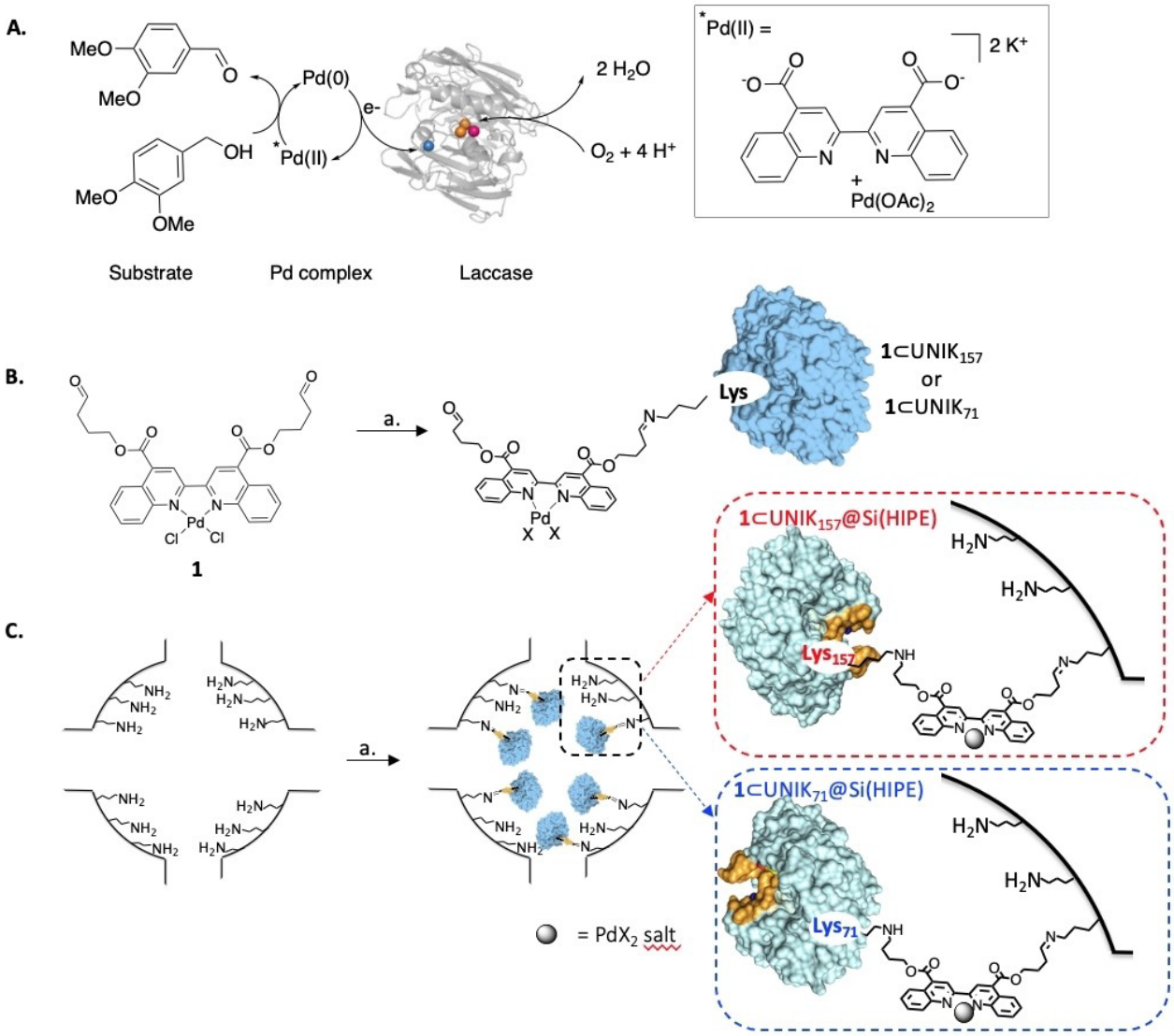

Scheme 1. A. Bimolecular synergistic interaction of a biquinoline Pd(II) based complex and a laccase to promote benign oxidation of veratryl alcohol into aldehyde. Laccase is reduced by a transient Pd(0) species and catalyzes the four-electron reduction of dioxygen into water with no loss of enzyme activity and integrity. Colored balls represent the copper centers. **B** and **C**. General strategy to produce immobilized **1**⊂UNIK hybrids Palladium (II) complex **1** is used for the covalent grafting of a UNIK variant by a reductive alkylation-based reaction (**B**). X = Cl or water. **a**. Reductive alkylation reaction. Post-functionalization of APTES functionalized Si(HIPE) foams (NH_2@Si(HIPE) is performed through Schiff-based forming reactions (**C**). **a**. Schiff-base forming reaction.

Table 1. Recovery yields, aldehyde quantification and specific activity for the **1**⊂$UNIK_{71}$ and **1**⊂$UNIK_{157}$ variants.

Enzyme	Yield %[a]	[Pd]/[T1 Cu(II)] UV-VIS	ICP-MS	SA U mg^{-1}[b] (Initial enzyme)
1⊂$UNIK_{71}$	85 ± 2	1.1 ± 0.1	1.1 ± 0.1	86 ± 2 (101 ± 3)
1⊂$UNIK_{157}$	89 ± 3	1.0 ± 0.1	1.1 ± 0.1	69 ± 4 (85 ± 2)

[a] Recovery yield estimated from the variation of the Cu(II) T1 absorption ($\varepsilon_{610nm} = 5.6 \times 10^3$ M^{-1} cm^{-1}) before and after functionalization. See Supporting Information for experimental details. [b] Laccase activity assayed at room temperature in 100 mM acetate buffer pH 5.7 using ABTS as substrate. One unit (U) of laccase is defined as one micromole of substrate oxidized per minute. The specific activity (SA) is defined as the number of unit (U) divided by the mass of laccase (mg). Extensive washing of solutions containing the UNIK variant ($UNIK_{71}$ or $UNIK_{157}$) and complex **1** with buffer (100 mM pH 5.7 acetate buffer) allows complete elimination of **1** (data not shown), attesting the absence of unspecific binding to the enzyme surface.

indicating that surface functionalization does not affect the copper centers (Figure 1B, Table S2). Altogether, these results confirm that reductive alkylation of UNIK variants result in single functionalizations of laccase surface that are not deleterious to the enzymes integrity.

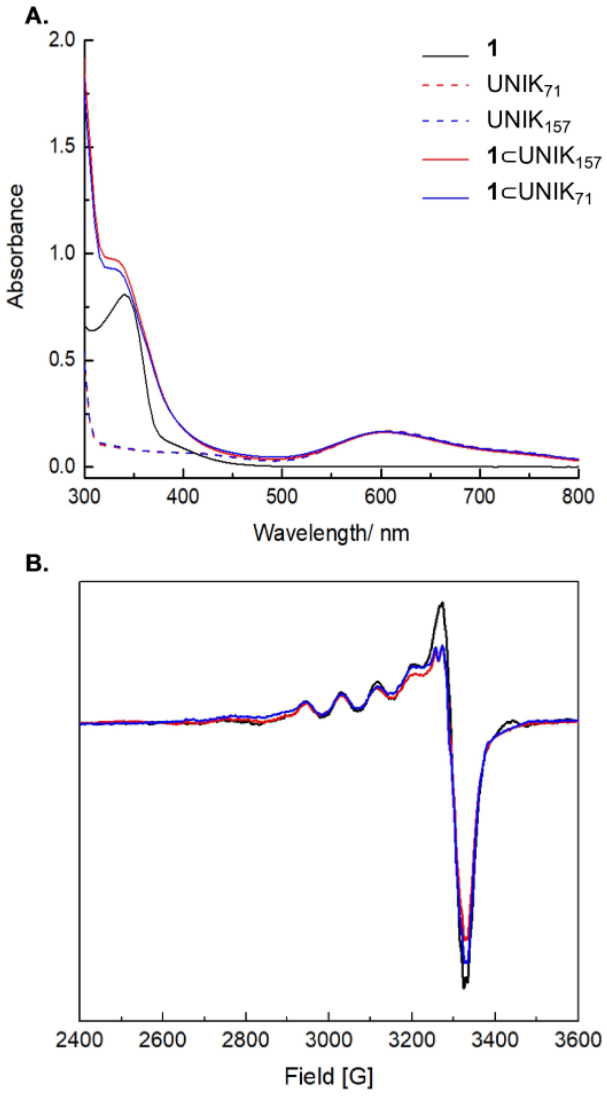

Figure 1. Spectral characteristic of hybrids. A. UV-Vis spectra of **1**, $UNIK_{157}$, $UNIK_{71}$ and their corresponding **1**⊂$UNIK_{157}$ and **1**⊂$UNIK_{71}$ hybrids in acetate buffer pH 5.7. B. X-band Electron spin resonance (ESR) spectra recorded from frozen solutions; (–) spectrum characteristic for one or the other UNIK variants; (–) **1**⊂$UNIK_{71}$; (–) **1**⊂$UNIK_{157}$ hybrids. Recorded at 115 K, microwave power 20 mW, modulation 3 G, gain 10^5.

Immobilization and characterization of the functionalized material

Based on our previous experience of laccase immobilization within macrocellular Si(HIPE) monoliths,[21] we proceeded to the immobilization of the two **1**⊂UNIK hybrids as well as complex **1** on APTES ((3-Aminopropyl)triethoxysilane) functionalized Si(HIPE) foams (designed as NH_2@Si(HIPE)) via a Schiff-based forming reaction between the free aldehyde moiety of the hybrid and the NH_2 moiety of the activated silica foam (Scheme 1C). We have previously shown that a covalent binding is mandatory to prevent leaching of the enzyme.[21] An effective covalent bond formation was challenged by performing extensive wash steps of monoliths in-line (3 mL min^{-1} unidirectional flow for 1 h) and successively with a high ionic strength buffer (1 M NaCl) and a chaotropic agent (1% Triton X100 in 100 mM acetate buffer) in order to disrupt any non-covalent interactions (hydrophobic or ionic) between hybrids and the material. This treatment did not lead to a detectable release of laccase. Thus, we conclude that the synthetic procedure leads to an efficient covalent attachment of the **1**⊂UNIKs hybrids to the silica surface.

Loadings of hybrids and complex **1** were initially evaluated by UV-Vis spectroscopy following the signature of the hybrid remaining in the impregnation solution and by measuring the metal content (Pd and Cu) by ICP-MS (Figure 2A, Table S3, S4). Pd(II) loads reached a maximum of $\sim 35 \times 10^{-6}$ mol g^{-1} of foam when working with an initial concentration of **1** $= 4 \times 10^{-3}$ mol L^{-1}. The yield of immobilized complex (amount of **1** bound/initial amount of **1**) ranged between 15–20%. As the diameter of complex **1** is estimated to be 10 Å from X-ray analysis, there is no limitation for the grafting of complex **1** into the macropores of Si(HIPE). The evolution of the Pd(II)-laccase hybrids binding as a function of the initial concentration of hybrids appears to be linear, with no apparent saturation (Figure 2A). The foam being constituted of macropores with polydisperse diameters at the μm length scale, this confirms a good material accessibility for hybrids. Yields of ca. 40–50% immobilization, were consistently obtained for both **1**⊂$UNIK_{71}$ and **1**⊂$UNIK_{157}$. Note that these immobilization yields are significantly higher than those we previously reported for the bare enzyme immobilization.[21] This may be due to the length of the grafting moiety (longer in this case), which could reduce steric hindrance.

Neo-synthetized grafted materials were further characterized by infra-red spectroscopy. Characteristic features such as C=O stretching modes at 1720 cm^{-1} and aromatic ring stretching modes at 1500–1400 cm^{-1}, 1200–1000 cm^{-1} and 900–700 cm^{-1} support the successful immobilization of complex **1** in NH_2@Si(HIPE) (Figure 2B, Table S5). For the immobilized hybrids, new peaks at 1637 cm^{-1} (C=N stretching band) and around 1540 cm^{-1} (amide II scissoring band) confirm the presence of laccase within the silica foam (Figure 2B). Solid state ^{29}SiNMR CP-MAS and ^{29}SiNMR MAS were used to characterize the nature of the silica support material at the molecular level (Figure S4, Table S6). Incompletely condensed Si species with a single residual hydroxyl group were found to represent ≈8% of the silicon atoms. This suggests an efficient grafting at the surface of the material. Therefore, the two immobilized hybrid catalysts are indistinguishable regarding their local Si environment.

Controlled by Scanning Electron Microscopy, macroscopic morphological features of the silica appear not affected by the presence of hybrids (Figure 2C). For all grafting (i.e. complex **1** and the two hybrids), the open porosity at the surface of the macroscopic wall (emerging from the starting emulsion coalescence feature) and the interstices between adjacent cells of the typical hollow spherical aggregated structure of the Si(HIPE) are still present.[19] Enzyme distribution within the silica foam was assessed by confocal microscopy using immunofluorescence staining (IFS) and by transmission electron microscopy (TEM) using immunogold staining (IGS) (Scheme S1). In both cases, the detection relies on the use of anti-laccase antibodies conjugated either to gold or to a fluorescent probe.[28] Silica

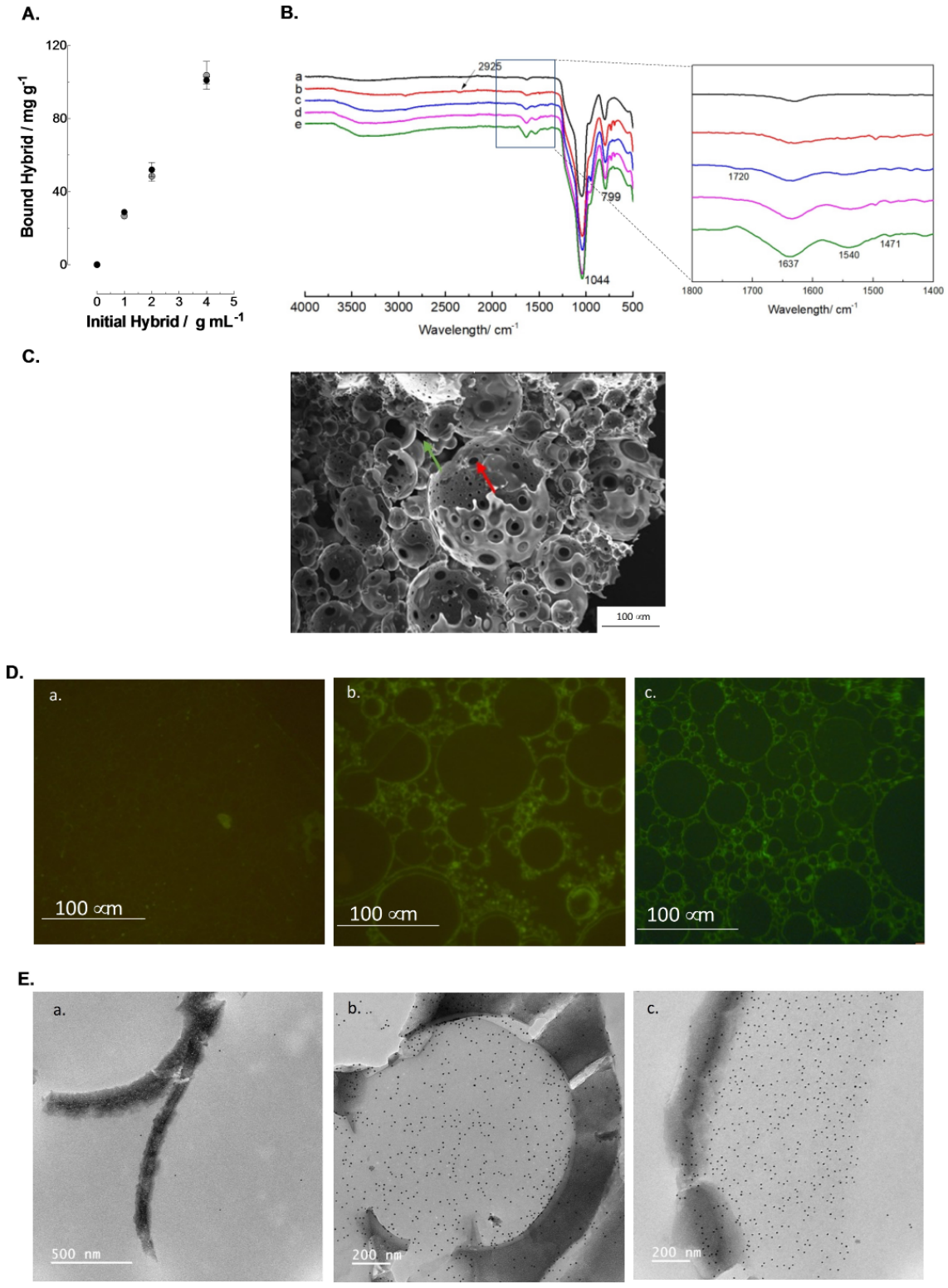

Figure 2. A. Hybrids loads into NH_2@Si(HIPE) as function of the initial hybrid concentration in the impregnation solution (see data in Table S4). ●**1**⊂UNIK$_{71}$ and ●**1**⊂UNIK$_{157}$. **B**. FT-IR spectra of (**a**) Si(HIPE) (**b**) NH_2@Si(HIPE) (**c**) **1**@NH_2@Si(HIPE) (**d**) **1**⊂UNIK$_{71}$@NH_2@Si(HIPE) and (**e**) **1**⊂UNIK$_{157}$@NH_2@Si(HIPE). The samples were dried in an oven at 80 °C overnight prior to analysis (see data in Table S5). **C**. SEM of **1**⊂UNIK$_{157}$@NH_2@Si(HIPE). Red arrow: intra-wall pore opening (internal junctions); green arrow: pore-opening from the hollow sphere aggregation (external junction). The sample was dried in an oven at 80 °C overnight prior to analysis. **D**. Confocal fluorescence microscopy images of sections (1 μm thick) revealed with primary rabbit anti-laccase antibody and donkey anti-rabbit IgG (H + L) cross-adsorbed secondary antibody, DyLight 488 of **a**. NH_2@Si(HIPE); **b**. **1**⊂UNIK$_{71}$@NH_2@Si(HIPE) and **c**. **1**⊂UNIK$_{157}$@NH_2@Si(HIPE. **E**. TEM immunogold labelling of ultrathin sections (80 nm thick) revealed with rabbit anti-laccase primary antibody and anti-rabbit secondary antibody conjugated with Au (Protein A-gold 10 nm): **a**. NH_2@Si(HIPE), **b**. **1**⊂UNIK$_{71}$@NH_2@Si(HIPE) and **c**. **1**⊂UNIK$_{157}$@NH_2@Si(HIPE). Loading of hybrid catalyst: 1.2×10^{-6} mol g^{-1} of foam. Note the presence of the laccase gold labeling (black spots).

materials with and without hybrid catalysts were embedded within a Lowicryl resin and cut into ultrathin sections (< 100 nm) that were in sequence incubated with a primary anti-laccase antibody (rabbit polyclonal antibody) and with a secondary antibody for detection (anti-rabbit gold or fluorescence Dylight 488 conjugated). Confocal microscopy fluorescence images of immuno-stained bare NH_2@Si(HIPE) and hybrid catalysts loaded foams are shown Figure 2D. The absence of fluorescence in control images (foams with no laccase, Figure 2D, panel a) attests for the absence of non-specific interactions between the antibodies and the silica foam. Images of **1**⊂$UNIK_{71}$@NH_2@Si(HIPE) and **1**⊂$UNIK_{157}$@NH_2@Si(HIPE) under 488 nm excitation reveal a green fluorescence that, in both cases, underlines the circumference of pores within the foam attesting the presence of the anti-LAC antibody and therefore of laccase (Figure 2D, panels b and d). Since laccase immobilization can be obtained only through a surface grafted Pd(II) complex **1**, localization of the enzyme supports a successful immobilization of complex **1** in the foam. Assessing qualitatively the green color intensity, no obvious difference was found regarding the immobilization of the two hybrids **1**⊂$UNIK_{71}$ and **1**⊂$UNIK_{157}$.

TEM images of immunogold labelling of foams loaded with hybrid catalysts and those of control samples are shown Figure 2E. In Si(HIPE) foam, the surface of pores is large and, at the magnification we used, TEM images cover only a fraction of a single macropore.[29] Images of NH_2@Si(HIPE) used as control tests are virgin of black spots and demonstrate the specificity of the process (Figure 2D, panel a). Images of foams functionalized with **1**⊂$UNIK_{71}$ or **1**⊂$UNIK_{157}$, contain black spots (Au^0 nanoparticles) homogeneously distributed (Figure 2E, panels b and c). Each black spot witness the presence of a laccase molecule and therefore hybrids. Laccase diameter is calculated to be roughly 67 Å (65 × 55 × 45 $Å^3$), a size perfectly suited for the macroporosity but not for the mesoporosity of Si(HIPE) ranging mostly from 2.5 to 1.5 nm. Comparing the classical morphology of Si(HIPE) with the size of the enzyme, as expressed before, the latter seem too large to fit within the mesoporosity, but simply line the macropores, appearing easily accessible without significant steric hindrance. In clear, all the catalytic sites observed in Figure 2 are stacked at the surface of the macropore surfaces but not embedded within the walls mesoporosity. As for fluorescence image, qualitatively, the density of gold particles in foams functionalized with either **1**⊂$UNIK_{71}$ or **1**⊂$UNIK_{157}$ appears similar in agreement with the calculated loads (Figure 2A). Altogether, the use of complementary IGS and TEM provides direct evidences on the presence and location of tandem catalysts inside the functionalized silica foams' macropore.

Catalytic performances

Homogeneous activity: One of the main challenges in chemo-enzymatic strategies is the potential for mutual deactivation of the tandem catalysts (metal and protein). Metallic and enzymatic catalysts usually require careful adjustment of reaction conditions in order to optimize their performance (solvent, reactant concentration).[30] In order to get the best cooperation between these two catalysts, a compromise must be found. We measured the activity of laccase towards ABTS in a buffer containing 5% DMSO, a solvent in which complex **1** is soluble. In the presence of 5% DMSO laccase variants $UNIK_{71}$ and $UNIK_{157}$ were found to retain ≈80% of their initial activity.

The model reaction employed for this study is the oxidation of veratryl alcohol (VA), a model compound for lignin degradation not oxidized by laccase (Scheme 1A). We have previously shown that: (*i*) LAC3 is reduced in the presence of a Pd complex and VA (bleaching of the T1 absorption band at 610 nm and disappearance of T1 and T2 ESR signatures), and (*ii*) after reoxygenation all the spectroscopic features indicative of reoxidation of laccase reappear. We initially controlled how the neo-synthetized complex **1** affects the redox states of the two laccase variants. Adding one equivalent of complex **1** in the presence of an excess of VA to a degassed solution of UNIK variants led to the complete reduction of their copper centers with similar kinetics ($t_{1/2}$ ca. 25 min) for each variant (Figure S5A, Figure S5B). When complex **1** is grafted at the surface of the enzyme, reduction rate appears up to two-times faster than in bimolecular conditions (**1**⊂$UNIK_{157}$: 12.5 ± 0.2 min; **1**⊂$UNIK_{71}$: 18.0 ± 0.2 min). Therefore, forming a covalent Pd/laccase complex favors the reduction of the copper centers of the enzyme compared to a simple bi-molecular solution probably by shortening the Pd–Cu centers distances. Possible routes for electrons may then include the surface grafted reduced complex **1** and either: i) the T1 copper or ii) the TNC. Both copper centers in UNIK variants can be efficiently reached by electron tunneling through the protein matrix.[27b,31,32] On the other hand, although working at low hybrid concentrations (50×10^{-6} M or less), an intermolecular ET occurring between a reduced complex **1** grafted on one hybrid and a copper center (either the T1 or the TNC) of another hybrid unit cannot be formally ruled out. Such a phenomenon has been observable in concentrated Ru–P450cam hybrid solutions.[33]

Performing the reaction in the presence of air, veratryl aldehyde (the product of the reaction) was found to accumulate in a time-dependent manner. The catalytic performances of hybrids **1**⊂$UNIK_{71}$ and **1**⊂$UNIK_{157}$ were first compared to the corresponding systems operated under bimolecular conditions at room temperature and in buffered water (Table 2). The activity of complex **1** alone (0.05‰) which oxidizes selectively veratryl alcohol into the corresponding aldehyde with a low efficiency (85 ± 0.1 10^{-6} M, 17.0 TON, 0.7 h^{-1} TOF) served as control (Table 2, entry 1). [If compared to the original Pd(II) biquinoline complex, complex **1** exhibits higher activity at lower loading.[23] (*i.e.* **1** (0.5‰): 5.0 TON, 0.2 h^{-1}).] As expected, incubation of equimolar ratio of UNIK variants and complex **1** (same concentration as in control) enhances the product formation that reached a maximum of 71 TON (3.0 h^{-1} TOF) for $UNIK_{71}$ and 62 TON (2.6 h^{-1} TOF) for $UNIK_{157}$ (Table 2, entry 2 and 3). In both cases, the presence of laccase led to a ca. 4-fold-increase of TON (check increased factor IF, in Table 2). Thus, as with the biquinoline Pd(II) complex we previously used [a strict comparison of the catalytic performance of **1** and Pd biquinoline complex previously published in presence of laccase is not

Table 2. Aerobic oxidation of veratryl alcohol in homogeneous conditions.

Entry	System[a]	Yield × 10^{-6} M	TON[b]	TOF (h^{-1})[c]	IF[d]
1	**1**	84.8 ± 1.0	17.0 ± 0.30	0.7	1.0
2	**1** + $UNIK_{71}$	354.4 ± 2.3	70.9 ± 0.50	3.0	4.2
3	**1** + $UNIK_{157}$	309.3 ± 0.1	61.9 ± 0.02	2.6	3.6
4	**1**⊂$UNIK_{71}$	413.1 ± 4.6	82.6 ± 0.90	3.4	4.9
5	**1**⊂$UNIK_{157}$	500 ± 28.0	100.2 ± 5.50	4.2	5.9

[1] = [UNIK] = [**1**⊂UNIK] = 5×10^{-6} M, [substrate] = 100×10^{-3} M in 100×10^{-3} M acetate buffer pH 5.7. 24 h catalysis at 25 °C. Results from triplicates. [a] $UNIK_{157}$ and $UNIK_{71}$ are not active toward veratryl alcohol oxidation. [b] TON calculated as the number of moles of product divided by that of the catalytic system and normalized with laccase specific activity. For the bimolecular system, the amount of catalyst refers to palladium complex. [c] TOF=TON per 24 h. [d] Increase Factor (IF) = TON of **1** in the presence of laccase/TON of **1**.

possible since conditions differ (enzyme, complex loading, co-solvent). As previously mentioned, the presence of 5% DMSO during the catalysis with **1** slightly alters the enzyme activity and may affect the efficiency of the synergistic effect], the ability of complex **1** to oxidize VA is greatly enhanced by the presence of laccase. Note that varying the ratio **1**/UNIK variant did not lead to an increase of the TON (Figure S6). Similarly, to their bimolecular systems counterparts, hybrids **1**⊂$UNIK_{71}$ and **1**⊂$UNIK_{157}$ were found performing 5–6 times better than complex **1** alone in the control experiment (Table 2, entry 4 and 5). This supports a preservation of the synergistic effect upon grafting. Aldehyde production increases with hybrid concentration, reaching a maximum of 650–700 × 10^{-6} M aldehyde (64.9 ± 2.49 TON and 70.21 ± 0.44 TON respectively for **1**⊂$UNIK_{71}$ and **1**⊂$UNIK_{157}$) at 10 10^{-6} M catalyst (Figure 3A). At the lowest hybrid concentration tested (1×10^{-6} M) TON's of 180 and 203 were respectively calculated for **1**⊂$UNIK_{71}$ and **1**⊂$UNIK_{157}$. As the concentration of hybrid increased, we noticed a parallel evolution of increase factors of both hybrids (Figure 3B). Therefore, under homogeneous conditions, location of the Pd(II) complex graft at the enzyme surface does not seem to significantly influence the reactivity of the hybrid. As already mentioned, this reflects that routes by which electrons reach the copper centers are not particularly discriminating. Not to mention that in the presence of both dioxygen and a highly reducing metal species (i.e. a Pd(0)), we must also consider the presence of a superoxide potentially playing the role of a redox mediator for the enzyme.[34]

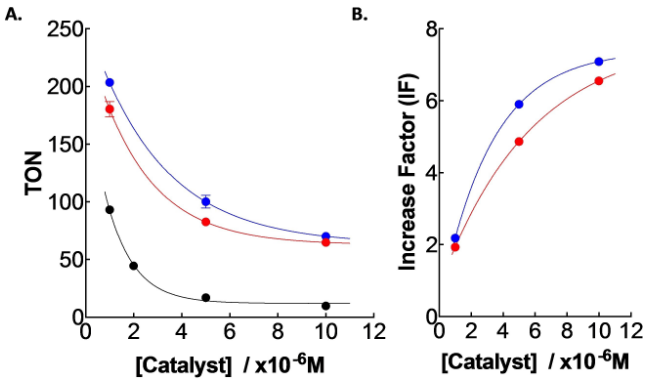

Figure 3. Veratryl alcohol oxidation by **1**⊂$UNIK_{71}$ and **1**⊂$UNIK_{157}$ grafted enzymes in homogeneous conditions. **A.** TON as function of catalyst concentration. TON are calculated as the ratio of moles of product to that of the catalyst and normalized with laccase specific activity. [substrate] = 100×10^{-3} M; [catalyst] = 1 to 10×10^{-6} M; t = 24 h, acetate buffer 100 mM pH 5.7 at 25 °C. °C. **B.** Increase factor (IF) as function of hybrid concentration in solution. IF is defined as the ratio of TON of TON **1**⊂UNIK or **1** + UNIK/TON **1**. λ **1**; λ **1**⊂$UNIK_{157}$; λ **1**⊂$UNIK_{71}$.

Heterogeneous activity: Veratryl alcohol oxidation was performed with hybrid materials **1**⊂$UNIK_{71}$@NH_2@Si(HIPE) and **1**⊂$UNIK_{157}$@NH_2@Si(HIPE) as well as with **1** @NH_2@Si(HIPE) used as control (Figure 4, S7, S8). Catalysts loads of 0.3, 0.6 and 1.2 × 10^{-6} mol g^{-1} for hybrids (and up to 35.2 × 10^{-6} mol g^{-1} for complex **1**) were tested in continuous flow conditions (50×10^{-3} g of foam, 15×10^{-3} L of mobile phase). In first analysis, (*i*) immobilization of complex **1** alone results in a heterogeneous catalyst with a measurable activity on VA and (*ii*) the synergy between laccase and complex **1** observed in homogeneous conditions is clearly preserved within the foam. TONs reached with immobilized hybrids are 4 to 8 times higher than that obtained with complex **1** alone (Figure 4). In the condition of an excess of substrate, product formation reaches a plateau at 24 h (Figure S8).

Comparing initial velocities at comparable loadings, immobilization of **1**⊂$UNIK_{157}$ appears advantageous as compared to **1**⊂$UNIK_{71}$ by a factor of 4 (Figure S8E). Yields increases similarly for each hybrid with loads up to 0.6 10^{-6} mol g^{-1} then decreases at twice this value (1.2×10^{-6} mol g^{-1}). Increasing loads densify the presence of hybrids within pore structure (see Figure 2E). This may lead to interactions amongst hybrids and, to a certain extent, favor hybrids performance at least up to a threshold above which crowding may affect hybrids efficiency. Such a behavior has been already observed with an immobilized laccase[21] as well with other enzymes as lipases.[35] In the case of the material we used, catalysis occurs at the macropores level where the surface area is considered as low.[19]

Interestingly, in heterogeneous conditions the performance of **1**⊂$UNIK_{157}$ is two times higher than that of **1**⊂$UNIK_{71}$, whatever the load of hybrid, underlining a significant effect of the orientation of hybrids at the silica matrix surface (Figure 4). As mentioned earlier, in homogeneous solutions, catalytic efficiency is not significantly affected by the location of complex **1** at the enzyme surface.

Within the foam, this effect only depends on the orientation of the enzyme relative to complex **1** both hybrids being immobilized at the same anchoring point (*i.e.* complex **1** aldehyde moiety). Therefore, not only does this immobilization method not compromise the performance of Pd/laccase

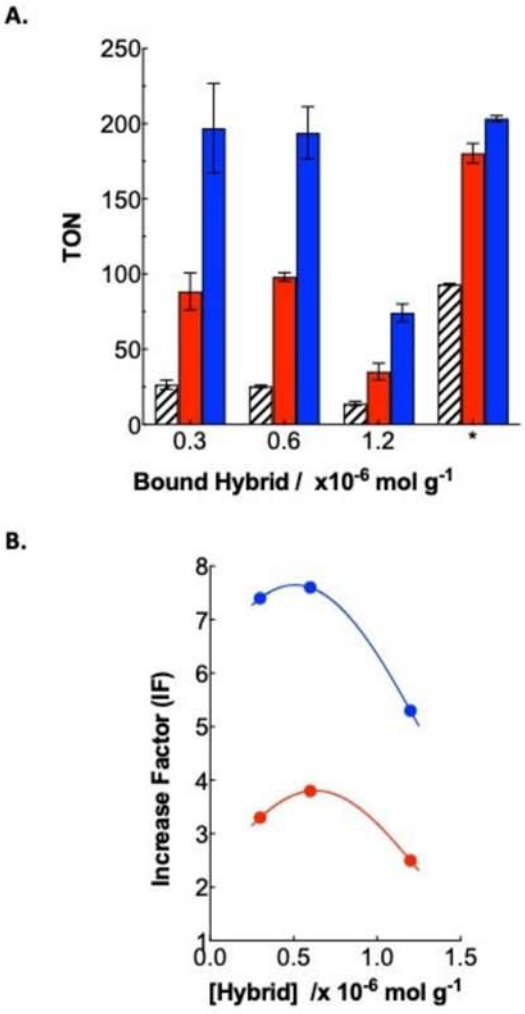

Figure 4. Veratryl alcohol oxidation as function of the catalyst load into the silica matrix. (**A**) Evolution of TON: **1**@NH_2@Si(HIPE) (dashed bars); **1**⊂$UNIK_{157}$@NH_2@Si(HIPE) (blue); **1**⊂$UNIK_{71}$@NH_2@Si(HIPE) (red); * results obtained in homogeneous conditions at a concentration of hybrid comparable to that in 0.3×10^{-6} mol g^{-1} load. (**B**) Increase Factor (IF) as function of hybrids loading: λ **1**⊂$UNIK_{157}$@NH_2@Si(HIPE); λ **1**⊂$UNIK_{71}$@NH_2@Si(HIPE). IF is defined as the ratio of TON of TON **1**⊂UNIK/TON **1**. Reactions performed with 50×10^{-3} g of grafted foams in 15×10^{-3} L of acetate buffer (100×10^{-3} M, pH 5.7) at 25 °C; [substrate] = 100×10^{-3} M; t = 24 h; 3×10^{-3} L min^{-1}.

hybrids, but it allows a distinction between **1**⊂$UNIK_{157}$ and **1**⊂$UNIK_{71}$ hybrids the specific activity of which differs by a factor of 2 within the foam. Best IFs are observed at 0.3 and 0.6 10^{-6} mol g^{-1} loads (Figure 4B). Unlike what is observed under homogeneous conditions, IF decreases with higher loads attesting probably a crowding effect. As shown by TEM (Figure 2E), hybrids (1.2 10^{-6} mol g^{-1}) are homogeneously distributed at the surface of the foam. It is conceivable that immobilization minimizes any intermolecular ET that could occur between hybrid units during catalysis, distances between neighboring hybrids units being probably too large at the optimal activity loads (e.g. 0.3–0.6×10^{-6} mol g^{-1}). Higher loads, in principle more favorable for intermolecular ET, were shown to alter the catalytic performance of each hybrid. Altogether, these results highlight a differential efficiency of the catalysts in relation to the localization of the Pd relative to the T1 Cu^{II} center in these hybrids (Scheme 2).

Reusability and stability: Generally speaking, immobilization is expected to contribute to the stabilization of catalysts and provide a mean for a recovery and a multiple utilization. Both immobilized hybrids (loads = 0.6×10^{-6} mol g^{-1}) were found indistinguishable regarding the reusability of the catalyst (Figure 5). After three initial consecutive cycles of VA oxidation including thorough in-place washing, 85–90% of the initial activity of catalysts was retained. At this stage, there was no indication of an instability of heterogeneous catalysts in the reaction conditions employed. In order to address thermodynamic stability on longer time-scale, stability and reusability were tested after a storage of wet foams at 4 °C (Figure 5). After 3 months of storage and one additional cycle, VA oxidation activity remained as high as 78% and 60% of the initial activity for the immobilized **1**⊂$UNIK_{71}$ and **1**⊂$UNIK_{157}$ catalysts respectively. After a total of 8 months of storage and five consecutive cycles, activities eventually dropped respectively to 40 and

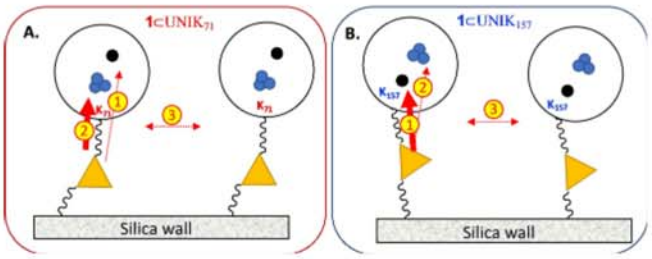

Scheme 2. Schematic representation of possible electron routes for laccase reduction in heterogeneous conditions. Route ① intramolecular complex **1** – T1 reduction; Route ②: intramolecular complex **1** – TNC reduction; Route ③: intermolecular T1 or TNC reduction. Plain arrow: more favorable. Dotted arrow: less favorable. Laccase variants: black circle; Complex **1**: orange triangle; T1 center: black bullet; TNC: three blue bullets.

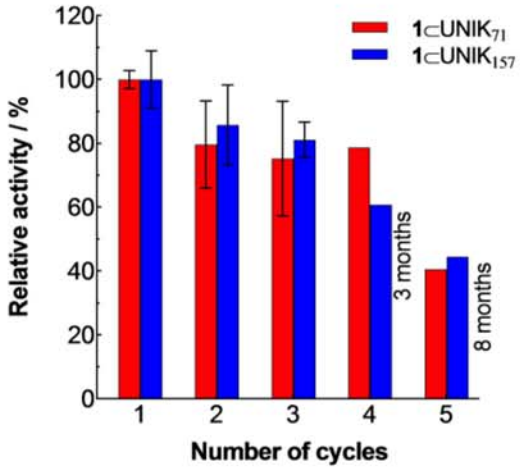

Figure 5. Evolution of the veratryl alcohol oxidation activity. of immobilized **1**⊂$UNIK_{71}$ and **1**⊂$UNIK_{157}$. Reaction in acetate buffer 100×10^{-3} M pH 5.7 at 25 °C [substrate] = 100×10^{-3} M; t = 24 hours for each cycle. Loading for **1**⊂$UNIK_{71}$ and **1**⊂$UNIK_{157}$ is 0.6×10^{-6} mol g^{-1}. Cycles 1 to 3 are consecutive 24 hours cycles. Cycles 4 and 5 were measured after 3 months and 8 months respectively.

44%. Whereas tested in similar conditions the activities of immobilized laccase variants (i.e. $UNIK_{71}$ and $UNIK_{157}$) were found to be stable for more than a year,[21] the stability of their supported Pd(II)-laccase hybrids counterparts was found diminished by ca. 50% after 8 months. This points out that palladium is a central element in the decrease in activity potentially through metal leaching.

Conclusion

We produced a chemoenzymatic catalysts built as a covalent hybrid between a laccase (enzymatic catalyst) and a palladium complex (metal catalyst) and further used a hierarchical silica foam as host for their co-immobilization. When confined at the macroscopic siliceous walls 'interface, hybrid catalysts conserve a veratryl alcohol oxidation activity. Compared to the basal activity of an immobilized palladium complex alone, that of immobilized hybrids is exalted, highlighting a synergy between the two catalytic partners in a confined environment. Globally, this technology allows to perform alcohol oxidation reactions under mild conditions, whereas addressing stable and reusable heterogeneous monolith catalysts. Interestingly, the catalytic performance can be modulated through the orientation of the enzyme relative to the functionalization localization. The Si-(HIPE)-Pd–T1 Cu(II) orientation reached with $\mathbf{1}\subset UNIK_{157}$ leads to 2 folds higher activity than that observed with the $\mathbf{1}\subset UNIK_{71}$ hybrid, a performance clearly exacerbated by the heterogeneous configuration. This suggests that the silica matrix might be more than a inert host allowing not only a dramatic stabilization (8 months) and a reuse of catalysts at ease through the confinement, but potentially a partner regarding the whole catalytic process (weak acidic pending silanol groups and/or associated hydration that may favor the enzymatic lubrication during several months). This work highlights the importance of controlling the spatial organization of catalytic partners (silica/Pd/laccase) under a heterogeneous hybrid configuration. At the molecular level, We demonstrate that it is possible to optimize catalysis performances by tuning the organization of immobilized Pd(II) and laccase catalysts acting in tandem, the whole heterogeneous catalyst providing both good cyclability, easy reusability and outstanding durability (up to 8 months).

Experimental Section

Tetraethyl-orthosilane (TEOS), tetradecyltrimethylammonium bromide (TTAB), dodecane and hydrochloric acid (37%), glutaradehyde Grade I 25% in H2O (wt.%) and (3-Aminopropyl)triethoxysilane (APTES) were purchased from Sigma. 2,2′-azino-bis(3-ethylbenzothiazoline-6-sulfonic acid (ABTS), veratryl alcohol from Fisher. All buffer solutions were made with deionized water. All other chemicals and reagents used in this study are of analytical grade and are used without any further purification. UNIK variants were expressed in *Aspergillus niger* and purified according to previously published procedures.[36] All instruments used are listed in the supplementary Information file.

Standard enzyme assay: Laccase activity was assayed at room temperature using ABTS as substrate. Oxidation of ABTS was detected by following the absorbance at 420 nm (ε 420 nm = 3.6 × 104 $M^{-1}cm^{-1}$) during 5 min. The reaction mixture (1 mL) contained 10 µL of appropriately diluted enzyme sample and 990 µL of 2.5 mM ABTS freshly prepared in acetate buffer (100 mM, pH 5.7). The enzyme was added to initiate the reaction. One unit (U) of laccase is defined as one micromole of substrate oxidized per minute in these described conditions. The specific activity (S.A.) is defined as the number of unit (U) divided by the amount of laccase (mg). The molecular weight of laccase is 84 kDa.

Ligand L synthesis: To 1.5 g (3.2 mmol) of 2,2′-Biquinoline-4,4′-dicarboxylic acid dipotassium salt trihydrate slurried in 40 mL DMSO, 1.85 g (9.5 mmol, 3 eq.) of 2-(3-Bromopropyl)-1,3-dioxolane were added at room temperature under N_2. The mixture was stirred at 40 °C in the dark for 26 h and then for additional 68 h at room temperature, after which it was quenched upon cooling with 200 mL of water. Then 200 mL CH_2Cl_2 were added to the mixture. The organic layer was separated and washed with water (3 × 100 mL) to remove the excess DMSO. The organic layers were combined, dried with Na_2SO_4 and evaporated to dryness. Recrystallization from CH_2Cl_2/Petroleum ether (10:1) yielded pure protected ligand (1.2 g, 56%) as a white solid. A solution of CAN (1.44 g, 2.6 mmol, 7.5 eq) in borate buffer (0.1 M, pH 8, 3 mL) was then added to a stirred solution (70 °C) of the protected ligand (200 mg, 0.35 mmol) dissolved in 6 mL acetonitrile. The resulting mixture was maintained under constant stirring for 20 min. Then 10 mL water were added to the mixture. After extraction with dichloromethane (3 × 20 mL), the combined organic layers were dried over $MgSO_4$ and the solvents are removed in vacuo. Pure **L** (150 mg, yield = 88%) was obtained without further purification. Characterization of the protected ligand and **L** were performed by NMR, ESI-MS and elemental analysis.

Complex 1 synthesis: 180 mg (0.371 mmol) of ligand **L** was added slowly to a solution of $PdCl_2(CH_3CN)_2$ (106 mg, 1.1 eq.) dissolved in 15 mL of dichloromethane. The mixture was maintained under stirring for 24 h and then concentrated to a small volume (1–2 mL). Precipitation was performed by the rapid addition of 50 mL Et_2O. A yellow solid **1** (200 mg, 80%) was obtained after centrifugation and dried in air with static vacuum. Characterization of **1** was performed by NMR, IR, ESI-MS and elemental analysis. Slow diffusion of diethylether into a saturated complex **1** solution in CH_2Cl_2 afforded crystal suitable for X-ray analysis.

Deposition Number 2174927 (for complex **1**) contains the supplementary crystallographic data for this paper. These data are provided free of charge by the joint Cambridge Crystallographic Data Centre and Fachinformationszentrum Karlsruhe Access Structures service.

Hybrid preparation: Reductive alkylation of primary amino groups was performed with an adapted procedure from Mac Farland and Francis using an Ir catalyst in the presence of formate as hydride donors.[26] With this process, aldehydes are not reduced. In a 10 mL round-bottomed flask, equipped with a magnetic stirring bar, 200 µL of a 625 µM laccase solution in buffer A (0.5 M sodium phosphate buffer pH 7.4 containing 50 mM sodium formate), 100 µL of a 5 mM complex **1** stock solution (4 eq.) in buffer A and 90 µL of 14 mM water stable $[Cp^*Ir(bipy)(H_2O)]SO_4$ complex (Ir catalyst) were combined, adjusting to a final volume of 2.5 mL with buffer A. The reaction was carried out for 72 h at 25 °C with permanent stirring. Prior to any treatment, the soluble fractions were analyzed by SDS-PAGE. Then the solution was loaded on a desalting column (Sephadex G25) pre-equilibrated with 100 mM acetate buffer pH 5.7 containing 100 mM NaCl. The fractions containing the enzyme were collected and loaded onto ultra-

filtration device for desalting and buffer-exchange, using 100 mM sodium acetate buffer pH 5.7. Yield (%) was determined as the amount of purified enzyme*100/initial enzyme. Hybrids were characterized by SDS-PAGE, ICP-MS, UV-Vis and EPR spectroscopies. Hybrids combining **1**/UNIK$_{71}$ and **1**/UNIK$_{157}$ are respectively named as **1**⊂UNIK$_{71}$ or **1**⊂UNIK$_{157}$.

Preparation of NH_2@Si(HIPE): HIPE stands for High Internal Phase Emulsion. Si(HIPE) monoliths were synthesized from Tetraethylorthosilane (TEOS), tetradecyltrimethylammonium bromide (TTAB), dodecane and hydrochloric acid (37%) with a protocol adapted from Carn et al.[19b] NH_2@Si(HIPE) synthesis and characterization is described in a recent paper from us.[21] The silica monoliths obtained from the previous steps (approximately 50 mg each) were immerged in a 25 mL toluene/APTES solution. Dynamic vacuum was applied to force the solution into the pores of the monoliths. Static vacuum was then maintained overnight. After impregnation, the monoliths were washed with distilled water for three times. The obtained monoliths were dried at 80 °C for 24 h in an oven. Characterization of materials was performed by IR, NMR and microscopy.

Complex 1 immobilization: A NH_2@Si(HIPE) monolith (about 50 mg) was immerged in 3 mL of complex **1** dissolved in DMSO at a desired concentration (higher than 100 μM). The mixture was placed under dynamic vacuum for 30 min and then under static vacuum overnight. Finally, the monolith was washed three times with DMSO (3 mL, 3×10 min) to remove the excess of unbound complex **1**. Complex **1** loading was calculated by subtracting the detected palladium in the residual and washing solution from the initial impregnation solution (based on the absorbance at 340 nm). The grafted Pd was confirmed by palladium quantification using ICP-MS. The immobilized complex is named as **1**@NH_2@Si(HIPE).

Hybrid immobilization: A NH_2@Si(HIPE) monolith (about 50 mg) is introduced in a mixture containing 3 mL of DPBS (Dulbecco's Phosphate Buffered Saline) buffer pH 7.0 and the hybrid (**1**⊂UNIK$_{71}$ or **1**⊂UNIK$_{157}$) at a desired concentration. The mixture was placed under dynamic vacuum for 30 min and then under static vacuum overnight. The materials were then washed three times with DPBS buffer solution (3 mL, 3×10 min) to remove the excess hybrid. Hybrid loading is calculated by subtracting the detected hybrid in residual and wash solution from the initial impregnation solution. The residual solution and wash solution were filtered before detecting concentration. The immobilized yield was further verified by the quantification of copper and palladium using ICP-MS. The resulting supported hybrid catalysts are respectively named as **1**⊂UNIK$_{71}$@NH_2@Si(HIPE) and **1**⊂UNIK$_{157}$@NH_2@Si(HIPE). Characterization of materials was performed by IR, NMR and microscopy.

Immunostaining detection and TEM sample preparation: Both the bare Si(HIPE), NH_2@Si(HIPE) **1**⊂UNIK$_{71}$@NH_2@Si(HIPE) and **1**⊂UNIK$_{71}$@NH_2@Si(HIPE) were first dehydrated for 1 h in successive dimethylformamide/water baths (1 bath at 50/50; 1 bath at 70/30; 1 bath at 90/10 and 3 baths at 100% dimethylformamide), evacuating the pillboxes to remove air from the silica to facilitate homogeneous inclusion of samples. For the inclusion in Lowicryl, successive baths are made by a mixture of Lowicryl K4 M/dimethylformamide (1 bath at 50/50; 1 bath at 70/30; 1 bath at 90/10 and 3 baths at 100% Lowicryl K4 M). The polymerization was done at 4 °C under UV lamp for 1 h. Sections of 80 nm were made with the ultramicrotome LKB 8800 for immunogold staining and TEM observation. Sections of 1 μm were made with the LKB 8800 ultramicrotome for fluorescence immunostaining and epifluorescence observation on Leica microscope. For the immunogold staining (IGS) method, the sections were saturated with PBS (Phosphate Buffer Saline) (10×, pH 7.4) containing 5% bovine serum albumin (BSA) for 1 h at room temperature to block non-specific binding of antibodies. Then, the sections were rinsed 5 times with PBS and incubated with a primary rabbit anti-laccase antibody (1/200) in 0.5% BSA-PBS for 2 h. After rinsing 5 times with PBS, the sections were incubated for another 2 h at room temperature with the secondary anti rabbit antibody conjugated with Au (Protein A-gold 10 nm), diluted (1/200) in 0.5% BSA-PBS. The sections were washed 5 times with PBS, then washed 5 times with distilled water and finally observed by TEM. For fluorescence immunostaining method, the procedure is similar. The secondary antibody used was a Donkey anti-Rabbit IgG (H + L) Cross-Adsorbed Secondary Antibody, DyLight 488. The sections were observed by fluorescence microscopy.

Alcohol oxidation assay: In a typical homogeneous condition experiment, oxidation of veratryl alcohol was performed in 2 mL tube at 25 °C with gentle constant shaking. Freshly prepared complex **1**, UNIK + **1** or **1**⊂UNIK$_{71}$ or **1**⊂UNIK$_{157}$ solution (0 to 10 μM) was incubated with veratryl alcohol (100 mM) in 1 mL 100 mM acetate buffer pH 5.7 for 24 h. With immobilized samples, the catalytic performance was performed with a recycling reactor.[21] 15 mL 100 mM veratryl alcohol in 100 mM acetate buffer, pH 5.7 was cycled with a flow rate set at 3 mL min^{-1} at room temperature. Before starting catalysis, pure buffer was applied for 30 min in the whole system to wash out any unbound catalyst. After each cycle, the column was disconnected and the system washed with ethanol then distilled water. Samples were collected for analysis after 1 h, 2 h, 4 h, 6 h, 8 h, 24 h. For both methods (Homogeneous and heterogeneous), samples were filtered through 0.22 μm then applied onto a C18 nucleosil column (300 A, 250*4.6 mm) after quenching with one volume of an acetonitrile solution containing 2 mM benzophenone as a standard for quantification. The alcohol and aldehyde concentrations were determined spectrophotometrically at 280 and 310 nm respectively from standard curves performed with commercial alcohol and aldehyde solutions.

All other characterization data, original spectra are provided in the Supporting Information. Additional references cited within the Supporting Information.[37–39]

Acknowledgements

The authors would like to thank the Chinese Scholarship Council, Frenchbic and ED250 doctoral school for financial support. The authors would like to thank Artemis Kosta and Hugo Le Guenno and the Microscopy Core Facility of IMM.

Conflict of Interests

The authors declare no conflict of interest.

Data Availability Statement

The data that support the findings of this study are available from the corresponding author upon reasonable request.

Keywords: covalent imprinted immobilization · flow catalysis · heterogeneous chemoenzymatic oxidation · laccase · palladium

[1] P. N. Arno Behr, *Applied Homogeneous Catalysis*, Wiley-VCH, Weinheim **2012**.
[2] a) A. N. Campbell, S. S. Stahl, *Acc. Chem. Res.* **2012**, *45*, 851–863; b) D. Wang, A. B. Weinstein, P. B. White, S. S. Stahl, *Chem. Rev.* **2018**, *118*, 2636–2679.
[3] C. Parmeggiani, F. Cardona, *Green Chem.* **2012**, *14*, 547–564.
[4] S. J. Lippard, *Nat. Chem. Biol.* **2006**, *2*, 504–507.
[5] R. A. Sheldon, J. M. Woodley, *Chem. Rev.* **2018**, *118*, 801–838.
[6] F. H. Arnold, *Angew. Chem. Int. Ed. Engl.* **2018**, *57*, 4143–4148.
[7] H. J. Davis, T. R. Ward, *ACS Cent. Sci.* **2019**, *5*, 1120–1136.
[8] Y. Wang, H. Ren, H. Zhao, *Crit. Rev. Biochem. Mol. Biol.* **2018**, *53*, 115–129.
[9] G. Zhan, P. Li, H. C. Zeng, *Adv. Mater.* **2018**, *30*, 1802094–1802102.
[10] a) E. Heuson, F. Dumeignil, *Catal. Sci. Technol.* **2020**, *10*, 7082–7100; b) D. P. Debecker, V. Smeets, M. Van der Verren, H. Meersseman Arango, M. Kinnaer, F. Devred, *Curr. Opin. Green Sustain. Chem.* **2021**, *28*, 100437–100443; c) X. Li, C. Fu, L. Luo, J. Ge, *Cell Reports Physical Science* **2022**, *3*, 100742.
[11] a) M. Filice, M. Marciello, M. d P Morales, J. M. Palomo, *Chem. Commun.* **2013**, *49*, 6876–6878; b) J. M. Naapuri, G. A. Åberg, J. M. Palomo, J. Deska, *ChemCatChem* **2020**, *13*, 763–769; c) J. M. Palomo, *Chem. Commun.* **2019**, *55*, 9583–9589; d) N. Losada-Garcia, A. Rodriguez-Otero, J. M. Palomo, *Catalysts* **2020**, *10*, 753–763; e) N. Losada-Garcia, A. Jimenez-Alesanco, A. Velazquez-Campoy, O. Abian, J. M. Palomo, *ACS Appl. Mater. Interfaces* **2021**, *13*, 5111–5124.
[12] a) T. Görbe, K. P. J. Gustafson, O. Verho, G. Kervefors, H. Zheng, X. Zou, E. V. Johnston, J.-E. Bäckvall, *ACS Catal.* **2017**, *7*, 1601–1605; b) K. P. J. Gustafson, T. Gorbe, G. de Gonzalo-Calvo, N. Yuan, C. L. Schreiber, A. Shchukarev, C. W. Tai, I. Persson, X. Zou, J. E. Backvall, *Chem. Eur. J.* **2019**, *25*, 9174–9179.
[13] a) J. Ge, J. Lei, R. N. Zare, *Nat. Nanotechnol.* **2012**, *7*, 428–432; b) X. Li, Y. Cao, K. Luo, Y. Sun, J. Xiong, L. Wang, Z. Liu, J. Li, J. Ma, J. Ge, H. Xiao, R. N. Zare, *Nat. Catal.* **2019**, *2*, 718–725.
[14] S. Gao, Y. Liu, L. Wang, Z. Wang, P. Liu, J. Gao, Y. Jiang, *ACS Catal.* **2021**, *11*, 5544–5553.
[15] a) K. Engström, E. V. Johnston, O. Verho, K. P. J. Gustafson, M. Shakeri, C.-W. Tai, J.-E. Bäckvall, *Angew. Chem. Int. Ed.* **2013**, *52*, 14006–14010; b) S. Moradi, Z. Shokri, N. Ghorashi, A. Navaee, A. Rostami, *J. Catal.* **2020**, *382*, 305–319; c) Z. Shokri, N. Azimi, S. Moradi, A. Rostami, *Appl. Organomet. Chem.* **2020**, *34*, e5899.
[16] a) Q. Wang, D. Astruc, *Chem. Rev.* **2020**, *120*, 1438–1511; b) S. Dutta, N. Kumari, S. Dubbu, S. W. Jang, A. Kumar, H. Ohtsu, J. Kim, S. H. Cho, M. Kawano, I. S. Lee, *Angew. Chem. Int. Ed.* **2020**, *59*, 3416–3422; c) Y. Wang, N. Zhang, E. Zhang, Y. Han, Z. Qi, M. B. Ansorge-Schumacher, Y. Ge, C. Wu, *Chem. Eur. J.* **2019**, *25*, 1716–1721; d) Y. Wu, J. Shi, S. Mei, H. A. Katimba, Y. Sun, X. Wang, K. Liang, Z. Jiang, *ACS Catal.* **2020**, *10*, 9664–9673.
[17] a) V. Smeets, W. Baaziz, O. Ersen, E. M. Gaigneaux, C. Boissière, C. Sanchez, D. P. Debecker, *Chem. Sci.* **2020**, *11*, 954–961; b) M. Van der Verren, V. Smeets, A. vander Straeten, C. Dupont-Gillain, D. P. Debecker, *Nanoscale Adv.* **2021**, *3*, 1646–1655; c) A. vander Straeten, A. Bratek-Skicki, L. Germain, C. D'Haese, P. Eloy, C. A. Fustin, C. Dupont-Gillain, *Nanoscale* **2017**, *9*, 17186–17192.
[18] S. Gao, Z. Wang, L. Ma, Y. Liu, J. Gao, Y. Jiang, *ACS Catal.* **2020**, *10*, 1375–1380.
[19] a) A. Roucher, M. Depardieu, D. Pekin, M. Morvan, R. Backov, *Chem. Rec.* **2018**, *18*, 776–787; b) F. Carn, A. Colin, M.-F. Achard, H. Deleuze, E. Sellier, M. Birot, R. Backov, *J. Mater. Chem.* **2004**, *14*, 1370–1376; c) A. Roucher, E. Roussarie, R. Gauvin, R. Jad, S. Gounel, C. Stines-Chaumeil, N. Mano, R. Backov, *Enzyme Microb. Technol.* **2019**, *120*, 77–83; d) N. Brun, A. Babeau Garcia, H. Deleuze, M. F. Achard, C. Sanchez, F. Durand, V. Oestreicher, R. Backov, *Chem. Mater.* **2010**, *22*, 4555–4562.
[20] J. M. Bolivar, J. M. Woodley, R. Fernandez-Lafuente, *Chem. Soc. Rev.* **2022**, *51*, 6251–6290.
[21] F. Yang, R. Backov, J.-L. Blin, B. Fáklya, T. Tron, Y. Mekmouche, *Biotechnol. Rep.* **2021**, *31*, e00645.
[22] a) T. Tron, *Encyclopedia of metalloproteins* (Eds.: R. H. Kretsinger, V. N. Uversky, E. A. Permyakov), New York: Springer **2013**, pp. 1066–1070; b) S. Riva, *Trends Biotechnol.* **2006**, *24*, 219–226.
[23] Y. Mekmouche, L. Schneider, P. Rousselot-Pailley, B. Faure, A. J. Simaan, C. Bochot, M. Réglier, T. Tron, *Chem. Sci.* **2015**, *6*, 1247–1251.
[24] A. Ates, A. Gautier, B. Leroy, J.-M. Plancher, Y. Quesnel, J.-C. Vanherck, I. E. Markó, *Tetrahedron* **2003**, *59*, 8989–8999.
[25] Y. Muranishi, Y. Wang, M. Odoko, N. Okabe, *Acta Crystallogr. Sect. C* **2005**, *61*, 307–310.
[26] a) J. M. McFarland, M. B. Francis, *J. Am. Chem. Soc.* **2005**, *127*, 13490–13491.
[27] a) N. Lalaoui, P. Rousselot-Pailley, V. Robert, Y. Mekmouche, R. Villalonga, M. Holzinger, S. Cosnier, T. Tron, A. Le Goff, *ACS Catal.* **2016**, *6*, 1894–1900; b) S. Gentil, P. Rousselot-Pailley, F. Sancho, V. Robert, Y. Mekmouche, V. Guallar, T. Tron, A. Le Goff, *Chem. Eur. J.* **2020**, *26*, 4798–4804; c) S. Gentil, C. Pifferi, P. Rousselot-Pailley, T. Tron, O. Renaudet, A. Le Goff, *Langmuir* **2021**, *37*, 1001–1011; d) V. Robert, E. Monza, L. Tarrago, F. Sancho, A. De Falco, L. Schneider, E. Npetgat Ngoutane, Y. Mekmouche, P. R. Pailley, A. J. Simaan, V. Guallar, T. Tron, *ChemPlusChem* **2017**, *82*, 607–614.
[28] M. Piras, A. Salis, M. Piludu, D. Steri, M. Monduzzi, *Chem. Commun. (Camb.)* **2011**, *47*, 7338–7340.
[29] P. Schmidt-Winkel, W. W. Lukens, P. Yang, D. I. Margolese, J. S. Lettow, J. Y. Ying, G. D. Stucky, *Chem. Mater.* **2000**, *12*, 686–696.
[30] a) F. Rudroff, M. D. Mihovilovic, H. Gröger, R. Snajdrova, H. Iding, U. T. Bornscheuer, *Nat. Catal.* **2018**, *1*, 12–22; b) S. Schmidt, K. Castiglione, R. Kourist, *Chem. Eur. J.* **2018**, *24*, 1755–1768.
[31] T. Lazarides, I. V. Sazanovich, A. J. Simaan, M. C. Kafentzi, M. Delor, Y. Mekmouche, B. Faure, M. Réglier, J. A. Weinstein, A. G. Coutsolelos, T. Tron, *J. Am. Chem. Soc.* **2013**, *135*, 3095–3103.
[32] a) M. Dagys, A. Laurynėnas, D. Ratautas, J. Kulys, R. Vidžiūnaitė, M. Talaikis, G. Niaura, L. Marcinkevičienė, R. Meškys, S. Shleev, *Energy Environ. Sci.* **2017**, *10*, 498–502 ; b) N. Lalaoui, M. Holzinger, A. Le Goff, S. Cosnier, *Chem. Eur. J.* **2016**, *22*, 10494–10500 ; c) A. de Poulpiquet, C. H. Kjaergaard, J. Rouhana, I. Mazurenko, P. Infossi, S. Gounel, R. Gadiou, M. T. Giudici-Orticoni, E. I. Solomon, N. Mano, E. Lojou, *ACS Catal.* **2017**, *7*, 3916–3923; d) C. H. Kjaergaard, F. Durand, F. Tasca, M. F. Qayyum, B. Kauffmann, S. Gounel, E. Suraniti, K. O. Hodgson, B. Hedman, N. Mano, E. I. Solomon, *J. Am. Chem. Soc.* **2012**, *134*, 5548–5551; e) A. Sekretareva, S. Tian, S. Gounel, N. Mano, E. I. Solomon, *J. Am. Chem. Soc.* **2021**, *143*, 17236–17249.
[33] J. Contzen, S. Kostka, R. Kraft, C. Jung, *J. Inorg. Biochem.* **2002**, *91*, 607–617.
[34] R. Farran, Y. Mekmouche, N. T. Vo, C. Herrero, A. Quaranta, M. Sircoglou, F. Banse, P. Rousselot-Pailley, A. J. Simaan, A. Aukauloo, T. Tron, W. Leibl, *iScience* **2021**, *24*, 102378.
[35] a) S. Arana-Peña, N. S. Rios, D. Carballares, C. Mendez-Sanchez, Y. Lokha, L. R. B. Gonçalves, R. Fernandez-Lafuente, *Front. Bioeng. Biotechnol.* **2020**, *8*; b) H. Zaak, E.-H. Siar, J. F. Kornecki, L. Fernandez-Lopez, S. G. Pedrero, J. J. Virgen-Ortíz, R. Fernandez-Lafuente, *Process Biochem.* **2017**, *56*, 117–123; c) L. Fernandez-Lopez, S. Garcia Pedrero, N. Lopez-Carrobles, B. Gorines, J. Virgen-Ortíz, R. Fernandez-Lafuente, *Enzyme Microb. Technol.* **2017**, *98*, 18–25.
[36] a) Y. Mekmouche, S. Zhou, A. M. Cusano, E. Record, A. Lomascolo, V. Robert, A. J. Simaan, P. Rousselot-Pailley, S. Ullah, F. Chaspoul, T. Tron, *J. Biosci. Bioeng.* **2014**, *117*, 25–27; b) V. Robert, E. Monza, L. Tarrago, F. Sancho, A. De Falco, L. Schneider, E. Npetgat Ngoutane, Y. Mekmouche, P. R. Pailley, A. J. Simaan, V. Guallar, T. Tron, *ChemPlusChem* **2017**, *82*, 607–614.
[37] S. Varghese, P. J. Halling, D. Häussinger, S. Wimperis, *J. Phys. Chem. C* **2016**, *120*, 28717–28726.
[38] a) G. E. Maciel, D. W. Sindorf, *J. Am. Chem. Soc.* **1980**, *102*, 7606–7607; b) E. Bayer, K. Albert, J. Reiners, M. Nieder, D. Müller, *J. Chromatogr. A* **1983**, *264*, 197–213.
[39] R. A. Martin, S. Yue, J. V. Hanna, P. D. Lee, R. J. Newport, M. E. Smith, J. R. Jones, *Philosophical Transactions of the Royal Society A: Mathematical, Physical and Engineering Sciences* **2012**, *370*, 1422–1443.

Manuscript received: March 24, 2023
Revised manuscript received: May 4, 2023
Accepted manuscript online: May 5, 2023